

Non- d^0 ferroelectricity from semicovalent superexchange in bismuth ferriteYang Shen ¹, Xiangang Wan,² Qingbiao Zhao,¹ Gang Li ^{3,*} and Chun-Gang Duan ^{1,4,†}¹Key Laboratory of Polar Materials and Devices, Ministry of Education, Department of Electronics, East China Normal University, Shanghai 200241, China²Department of Physics and National Laboratory of Solid State Microstructures, Nanjing University, Nanjing 210093, China³School of Physical Science and Technology, Shanghai Tech University, Shanghai 201210, China⁴Collaborative Innovation Center of Extreme Optics, Shanxi University, Taiyuan 030006, Shanxi, China

(Received 6 March 2021; accepted 26 April 2021; published 15 July 2021)

Empirical d^0 rule, i.e., magnetic unpairing d occupation tends to be chemically incompatible for ferroelectrics, has for long inhibited the availability of room-temperature single-phase multiferroics. Here, we readdress the ferroelectricity of type-I multiferroic BiFeO₃, and conclusively clarify hybrid origins of lone-pair electrons' instability. Surprisingly, the sole lone-pair mechanism cannot account for overall polarization. Thus, beyond the popular belief, we propose that, with half-filling $t_{2g}^3 e_g^2$ configuration and stereochemical activity of Bi's lone pair preparticipating, renormalized nonempty Fe 3d orbitals render BiFeO₃ a strong p - d charge-transfer insulator, and further induce non- d^0 ferroelectricity through antiferromagnetic semicovalent superexchange. The magnetolectric coupling scenario is numerically elaborated by mean-field p - d model, and first-principles generalized gradient approximation GGA + U calculations. The magnetically induced ferroelectricity also reconciles the competitiveness of octahedral rotations and ferroelectricity, which turns into cooperative behavior as octahedral rotations straighten the Fe-O-Fe bonds and strengthen superexchange interactions. Such mechanism is in principle ubiquitous in magnets with superexchange interaction and manipulatable to hybridization engineering.

DOI: [10.1103/PhysRevB.104.024421](https://doi.org/10.1103/PhysRevB.104.024421)**I. INTRODUCTION**

The homotopy of polarization (\mathbf{P}) and magnetism (\mathbf{M}) in Landau's phenomenology and entanglements of the simultaneous ferroics promise technological applications and spawn dramatic academic interests [1–20]. Cores of sizable magnetoelectric coupling in multiferroics are the access to improper ferroelectricity where electric dipoles are nontrivially induced by magnetism. The scarcity of room-temperature multiferroics other than representative BiFeO₃ (BFO) [11,21], however, frustrates state of the art applications and precipitates a ferroelectric (FE) “ d^0 mystery” [22]: the magnetic partial- d occupation tends to be chemically incompatible for ferroelectrically active B -site transition metal (TM) with formal d^0 configuration in traditional ABO_3 perovskite oxides, e.g., ferroelectrics BaTiO₃, KNbO₃, and Pb(Zr _{x} Ti _{$1-x$})O₃. The empirical argument on such noncoexistence of magnetism and ferroelectricity is usually rationalized by pseudo Jahn-Teller (PJT) effect [23,24], wherein the covalent polar instability efficiently occurs via vibronic hybridization between ground (e.g., O $2p$) and unoccupied excited states (e.g., B $3d^0$) of same spin and opposite parity with the narrower the better charge-transfer gap Δ_{CT} . Within this scenario, traditional wisdom ascribes the ferroelectricity in BFO to Bi's outmost $6s$ lone-pair electrons, which feature asymmetric lobe shapes in real space, and spontaneously break space-inversion symmetry via electron-phonon coupling. BFO is

consequently reckoned as type-I multiferroic with separate polar and magnetic origins, and endowed with weak magnetolectric coupling. However, extraordinarily large \mathbf{P} (versus d^0 lone-pair ferroelectric PbTiO₃) and concurrent \mathbf{P} and \mathbf{M} enhancement in BFO [18,25] is at odds with the exclusive multiferroicity in individual sublattices and defies the sole lone-pair FE mechanism [11,26,27]. In principle, magnetic cations are also capable of PJT FE distortions, which reconciles the mutual exclusion [24,28–30]. Nevertheless, the thoughts on symmetry-allowed molecular orbitals in magnetic manifolds without specific interplays of electron correlation and magnetism cannot produce a realistic magnetically driven ferroelectricity.

As is well known, ferroelectric phenomenon occurs as the condensation of boundary-optical phonon resulting from the compensation of short-range repulsions by attractive long-range dipole-dipole interactions [31–35]. The PJT vibronic hybridization between B's $3d$ and O's $2p$ states reduces such short-range repulsions and the resultant p - d covalent energy gain drives charged ions off centricity towards ferroelectrics, with the formation of polarized covalent bonds. On the other hand, chemical bonds are created by overlaps of bonding wave functions with antiparallel spin orientations, that is, spin-singlet states $\frac{1}{\sqrt{2}}(d \uparrow p \downarrow - d \downarrow p \uparrow)$. On this level, there are intrinsic relationships among chemical bonds, magnetism (especially antiferromagnetism), and ferroelectricity. In magnetic contexts, exchange interaction can indeed facilitate such spin-singlet states and produce ferroelectricity. To clarify this, we compare two different situations for the virtual p - d hopping processes, which depend on electronic configurations and ultra(intra)orbital interactions [Fig. 1(a)].

*ligang@shanghaitech.edu.cn

†cgduan@clpm.ecnu.edu.cn

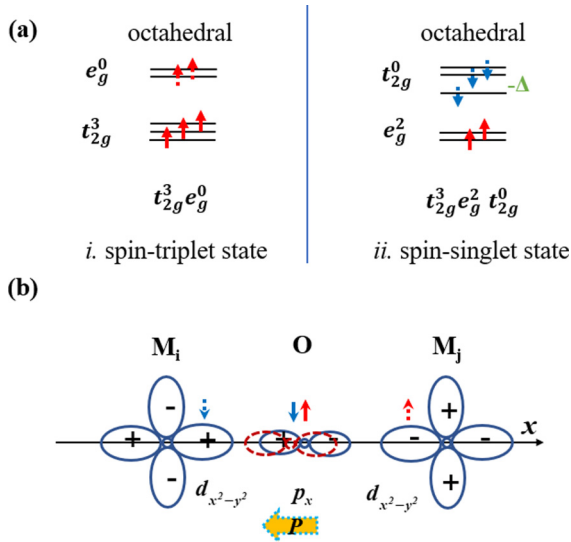


FIG. 1. (a) Schematic electronic level diagram in two cases: (i) J_H dominates in $t_{2g}^3 e_g^0$ manifold, with ferromagnetic coupling between highest occupied t_{2g}^3 and lowest unoccupied e_g^0 states, favoring spin-triplet states, and (ii) U dominates in $t_{2g}^3 e_g^2 t_{2g}^0$ manifold (remove spin degeneracy), with antiferromagnetic coupling between highest occupied e_g^2 and lowest unoccupied t_{2g}^0 states, favoring spin-singlet states with energy gain $-\Delta$. The solid arrows denote spin occupations and dotted arrows denote the virtual exchange-hopping processes in unoccupied orbitals (related oxygen $2p$ orbitals are not shown). (b) Illustration of longitudinal ferroelectricity (characterized by off-centric diamagnetic bridging anion) from indirect 180° magnetic superexchange interaction.

When Hund coupling J_H dominates, $3d$ orbitals prefer parallel spin arrangements and the virtual exchange p - d pairing creates spin-triplet states, which are destructive to FE instability and result in a magnetic paraelectric state. It is the case for $t_{2g}^3 e_g^0$ Mn^{4+} [23,36], wherein the strong ferromagnetic Hund's coupling with the localized t_{2g}^3 electrons acts as a “pair breaker” on the singlet state. However, the situation of Fe $3d^5$ manifold is completely different. Due to crystal-field splittings and electron correlation U , spin degeneracy is removed, and highest occupied and lowest unoccupied energy levels are $e_g^2 \uparrow$ and $t_{2g}^0 \downarrow$, respectively. As a result, the virtual exchange p - d pairing in superexchange mechanism may otherwise create antiferromagnetic p - d singlet state. As also for strong indirect exchange interaction, interatomic hybridization between magnetic and diamagnetic ions broadens bandwidth and narrows Δ_{CT} , to the extreme of FE instability under the configuration of exchange p - d pairing. Precisely, our previous work reveals that magnetic superexchange is enhanced in off-centric M_i -O- M_j alignment and thus unstable against a FE displacement [Fig. 1(b)] [37]; one can alternatively check the curvature (versus r_{pd}) of superexchange energetic potential $\sim -\frac{t_{pd}^4}{U\Delta_{\text{CT}}^2}$ [38] with the hopping $t_{pd} = Cr_{pd}^{-l}$ ($l > 0$) [39] is negative at arbitrary symmetric site r_0 , *viz.*, phonon instability. This way, the interatomic superexchange already provides a driving force towards ferroelectricity, besides Bi's lone pairs and regardless invoking weak relativistic Dzyaloshinskii-Moriya interaction in BFO [40–42]. We demonstrate that this effect is dominantly

operative in strong p - d charge-transfer insulators (wherein the exchange mechanism is properly termed as semicovalent superexchange [43]), to which BFO belongs [21].

Thus, in this paper, we readdress the origin of ferroelectricity in BFO, especially the symmetric superexchange magnetoelectric scenario beyond relativistic Dzyaloshinskii-Moriya interaction. In steps towards this, we first revisit the microscopic origin and traditional ferroelectricity of A site's lone pairs, which originate from nominal $ns^2 np^0$ electrons' instability with strong hybridizations among Bi's $6s$ and $6p$ as well as O's $2p$ states. We identify the microscopic origins via phonon frequencies of particular distortion modes and real-space mapping analysis of charge density and wave functions. The calculated polarization from lone pairs, however, cannot account for the overall polarization in BFO and contributions from magnetic Fe sites should be taken into consideration. Furthermore, we demonstrate the ferroelectricity from semicovalent superexchange mechanism in mean-field p - d model, which relies on strong trend of antiferromagnetic pairing with ligands (*i.e.*, the formation of spin-singlet states), and is consistently inspected within multiorbital generalized gradient approximation (GGA) + U calculations. We emphasize that the stereochemical activity of Bi $^{3+}$ $6s$ [2] lone pairs, manifesting in off-centric displacements in BiO $_2$ cage, rescales the Fe-O hybridization through nonbonding structural effects and triggers strong superexchange interaction in narrow charge-transfer regime. The semicovalent superexchange mechanism also reconciles the typical competitiveness of octahedral rotations and ferroelectricity, as octahedral rotations foster magnetic interaction by straightening Fe-O-Fe bonds and enhance the magnetically driven ferroelectricity. We thus conclusively clarify the ferroelectric origin in BFO and propose a prevailing magnetoelectric coupling mechanism in strong charge-transfer regime, which is manipulatable to hybridization engineering.

II. METHODOLOGY

The density-functional theory (DFT) method is performed for structural relaxation, magnetic constraints, and electronic structure calculations in the plane-wave basis with projector-augmented wave potentials [44,45], as implemented in the Vienna *Ab initio* Simulation Package (VASP) [46]. The exchange-correlation functional is treated within the scheme of GGA following Perdew-Burke-Ernzerhof prescription [47]. Strong electron-electron correlation beyond GGA for transition-metal oxides is supplemented by plus Hubbard U (GGA + U) calculations with Dudarev's approach [48]. An energy cutoff of 500 eV for the plane-wave expansion and a $7 \times 7 \times 7$ Monkhorst-Pack grid for k -point sampling are adopted for self-consistent calculations with good convergence. The symmetry-constrained structures were relaxed until the Hellmann-Feynman force on each atom was less than $1 \text{ meV } \text{\AA}^{-1}$. The Born effective charge was calculated by density-functional perturbation theory [49,50]. The electric polarization was obtained using the Berry phase method [51–53]. The phonon spectrums of paraelectric R $\bar{3}c$ BFO was calculated using the PHONOPY code [54]. The maximally localized Wannier functions (MLWFs) are interpolated by the postprocessing tool WANNIER90 [55], and plots of atomic

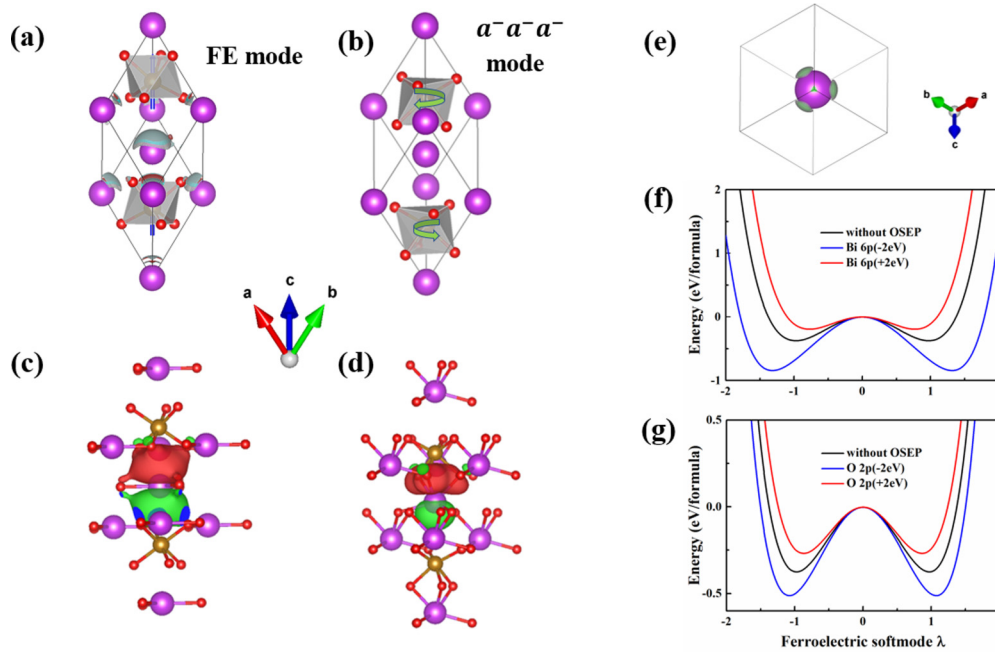


FIG. 2. Hybrid origins and ferroelectricity of lone-pair electrons. Schematization of (a) FE and (b) antiferrodistortive modes, respectively, in BFO. The lobelike charge isosurfaces near the Bi atom in (a) denote lone-pair electrons with FE mode. Bi's $6s-6p$ hybrid MLWFs along the (111) polar axis for (c) $R\bar{3}c$ and (d) $R3c$ structures, respectively. (e) Threefold rotational symmetry of Bi's charge distributions imposed by antiphase rotation mode. GGA + U double-well potential profiles with different external potentials on (f) Bi $6p$ and (g) O $2p$ orbitals.

structures, charge densities, as well as wave functions were elaborated with VESTA [56].

The orbital selective external potential (OSEP) method [57–60] is used to apply an external potential to shift the energy level of a specific atomic orbital, which in effect alters energy difference between orbitals, particularly bare charge-transfer energy gap Δ_{pd} , and to unambiguously clarify the contribution from entangled orbitals. The OSEP method is analogous to the GGA + U method in the sense that the applied potential is orbital dependent and only certain specified orbitals are exclusively affected via a projector operator $|inlm\sigma\rangle\langle inlm\sigma|$, wherein i denotes the atomic site, and n , l , m , σ are, respectively, the main quantum number, orbital quantum number, magnetic quantum number, and spin index. The new Kohn-Sham equations with certain orbital selective external potentials are solved in a self-consistent way encoded in VASP sources.

III. RESULTS AND DISCUSSION

A. Ferroelectricity of lone-pair electrons

Cations with a nominal ns^2np^0 electronic configuration, termed as lone-pair electrons, have been long known to cause Jahn-Teller distortions [61], large nonlinear optical responses [62], and ferroelectricity [63,64]. However, microscopic understandings of lone pair and its properties are still not fully established. As popular beliefs, lone-pair electrons are derived from $s-p$ orbital hybrids in noncentrosymmetric systems, which are otherwise forbidden due to $s-p$ parity confinement at centrosymmetric sites, and generate ferroelectricity as a PJT instability: the degeneracy of excited p orbitals is removed to meet hybridization requirements and gain energy from symmetry-lowering distortions [27]. Phenomenologi-

cally, orientations of these lone pairs, or dangling bonds, may create local dipoles, which can order in a complex pattern, such as (anti-)FE or noncollinear arrays [65]. Thus, ns^2 lone-pair ions are favorable for functionality of polarity.

We systematically explore microscopic formation of lone pair and its roles in ferroelectricity for BFO. As shown in Figs. 2(a) and 2(b), $R3c$ BFO lattice inherits perovskite ABO_3 with structural distortions (i) collective FE displacements along the pseudocubic (111) direction and (ii) antiphase oxygen octahedral FeO_6 rotations about the (111) direction (nonpolar, $a^-a^-a^-$ pattern in Glazer's notation). According to symmetry condition, lone pairs are associated with collective FE modes [Fig. 2(a)]. Noteworthy, the morphology of lone pairs is also counterbalanced by antiphase rotation mode, which imposes threefold rotational symmetry on Bi's charge distributions [Fig. 2(e)]. To determine the status of electronic hybridization, hybrid orbitals of paraelectric $R\bar{3}c$ and $R3c$ lattice structures are plotted as MLWFs in Figs. 2(c) and 2(d), respectively. The $R\bar{3}c$ BFO belongs to D_{3d} point group and the Wyckoff position of Bi atoms has $-3m$ site symmetry. Since s - and p orbitals transform as different irreducible representations of $-3m$, Bi $6s-6p$ hybridization is forbidden by symmetry and one of four MLWFs of Bi $6s-6p$ hybrid orbitals displays nonbonding p -like states along the threefold axis. For FE $R3c$ structure, the inversion and mirror site symmetries are removed, Bi $6s-6p$ hybridization is allowed and the Wannier functions of Bi $6s-6p$ hybrid orbitals display asymmetry shapes with mixed $6s$ and $6p$ components as charge density. Similarly, Wannier functions of O $2p$ orbitals also distorted to meet the s parity (not shown). Thus, lone pairs in FE BFO are formed by hybridizations among Bi's $6s$ and $6p$ as well as O's $2p$ states. Since the strength of hybridization between two orbitals strongly depends on

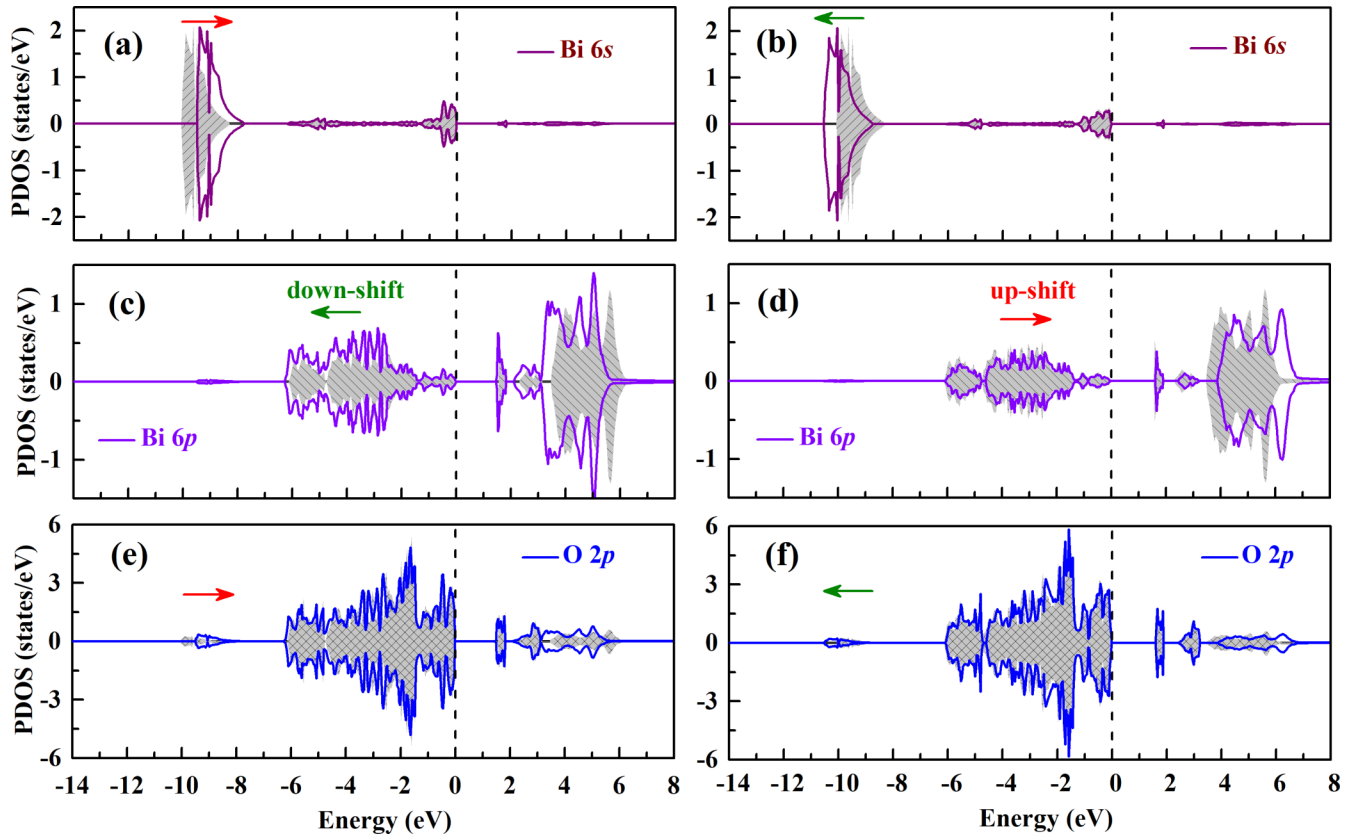


FIG. 3. PDOS for (a), (b) Bi $6s$, (c), (d) Bi $6p$, and (e), (f) O $2p$ with down-(left) and up-(right) shifting Bi's $6p$ states by 2 eV in $R3c$ BFO. The green and red arrows denote the corresponding down- and up-shift of electronic states, respectively. The Fermi level is set at zero energies (vertical dashed lines), and pristine PDOS are depicted as patterned plots.

their energy difference, we can further identify contributions of relative orbitals to lone pairs by shifting Bi's $6p$ and O's $2p$ states using OSEP method, wherein up(down)-shifting Bi's $6p$ and O's $2p$ states in(de)-creases energy differences versus Bi's $6s$ states. The projected density of states (PDOS) in Fig. 3 demonstrates the results when we shift Bi's $6p$ states (similar for shifting O's $2p$ states). Down(Up)-shifting Bi's $6p$ states directly moves the Bi's $6p$ states towards lower(higher) energy in the PDOS [Figs. 3(c) and 3(d)], and correspondingly, Bi's $6s$ and O's $2p$ states move towards higher(lower) energy, indicating the enhanced(weakened) hybridization among Bi's $6s$ and $6p$ as well as O's $2p$ states again, and also showing that OSEP method can indeed alter energy differences between orbitals. To clarify the instability of $6s^2$ electron, we calculate the phonon spectra of paraelectric $R\bar{3}c$ BFO (without emergent lone pairs) with down(up)-shifted orbitals and extract imaginary frequencies of FE soft mode. As shown in Table I, with down(up)-shifting Bi's $6p$ orbitals, the FE soft mode is enhanced (weakened) as compared with pristine $R\bar{3}c$ BFO without external potentials, signifying instrumental role of Bi $6s$ - $6p$ hybridization in the formation of lone pairs and its ferroelectricity. The FE soft mode displays similar results for shifting O's $2p$ states. The reciprocity can be self-evident with up (down)-shifting Bi $6s$ states due to the underlying hybridization (not shown). We also use λ method to describe FE instability characteristic of spontaneous symmetry-breaking soft modes, wherein the interpolation parameter $\lambda = +1$ and

-1 correspond to the polarization "up" and "down" states, respectively [66]. The potential profiles of normalized collective displacements in Figs. 2(f) and 2(g) feature a FE double-well potential, and FE magnitude is also in(de)-creased with deep(shallow) double well when down(up)-shifting Bi's $6p$ and O's $2p$ states, respectively. Therefore, we conclude that the electronic instability of ns^2 lone pair, i.e., stereochemical activity, drives the system towards ferroelectricity through electronic hybridization among Bi's $6s$ and $6p$ as well as O's $2p$ states, wherein the hybridization reduces short-range repulsions for the occurrence of long-range FE correlation. Surprisingly, the polarization induced by lone pairs in BFO is estimated as $\sim 47 \mu\text{C}/\text{cm}^2$, which cannot account for the overall polarization in BFO ($\sim 100 \mu\text{C}/\text{cm}^2$) and contributions from magnetic atoms remain to be invoked.

TABLE I. Imaginary frequencies of FE soft mode with different external potentials on Bi's $6p$ and O's $2p$ orbitals.

External potentials (eV)	Pristine (THz)	Bi $6p$ (THz)	O $2p$ (THz)
-2		-6.16	-6.07
0	-5.67		
2		-5.3	-5.24

B. Model Hamiltonian

To demonstrate the ferroelectricity from semicovalent superexchange mechanism, we study interplays of magnetic correlation, orbital hybridization, and FE instability in the single-band p - d model with explicit elastic energy $H = H_0 + H_\kappa$ for longitudinal displacive O in Fe₁-O-Fe₂ cluster [37]:

$$H_0 = \sum_{\sigma,i=1,2} \varepsilon_d c_{d_i\sigma}^+ c_{d_i\sigma} + \sum_{\sigma} \varepsilon_p c_{p\sigma}^+ c_{p\sigma} + \sum_{\sigma,i=1,2} t_i (c_{d_i\sigma}^+ c_{p\sigma} + \text{h.c.}) + \frac{U}{2} \sum_{\sigma,i=1,2} n_{i\sigma} n_{i\bar{\sigma}}, \quad (1a)$$

$$H_\kappa = N \times \frac{1}{2} \kappa \varphi^2. \quad (1b)$$

Herein ε_d (ε_p) denotes the on-site energy for the FE-active Fe t_{2g}^* ($O\ 2p$) manifold, t_i is the hopping integral, U is the Hubbard energy, and σ and i are spin and site indices, respectively. For H_κ , we adopt parametrizations $\kappa = kl^2 / (\frac{\partial \ln t}{\partial \ln l})^2$ and $\varphi = \frac{\partial \ln t}{\partial \ln l} \times \frac{\delta l}{l}$, where k denotes spring stiffness constant and l bond length of Fe-O [67]. The bridging O atom's orbital in the cluster is further eliminated based on standard Schrieffer-Wolff transformation [68], and the effective asymmetric p - d hopping integral (featuring ferroelectricity) between neighboring Fe³⁺ atoms yields:

$$t_{\text{eff}} = \frac{t_1(1 + \delta - \varphi) \times t_2(1 + \varphi)}{\varepsilon_d - \varepsilon_p}, \quad (2)$$

which describes the characteristics of $\pm\varphi$ staggered hybridization wave mediated by FE distortion [67]. In the paraelectric phase, $\varphi = 0$, and δ represents the asymmetry of hopping integral in Fe₁-O-Fe₂ cluster losing inversion center, reproducing nonlinear hopping t dependence on distances and ferroelectricity's displacive anharmonicity.

We calculate the phase diagram of the Hamiltonian H using self-consistent mean-field theory in the minimal antiferromagnetic bipartite lattice [69]. This mean-field approach ignores correlated density fluctuations; nevertheless, it adequately captures magnetic interactions. We work in units with $t_1 = t_2 = t = 1$. The dimensionless parameters δ and φ are chosen to be 0.1 and 0.2. The antiferromagnetic setup is achieved by tuning Fe sites' unbalanced spin-up/down occupancy numbers. Some variation in these parameters does not qualitatively affect our main results. Figures 4(a) and 4(b) show the ground-state phase diagram with varying bare charge-transfer energy gap Δ_{pd}/t and stiffness κ/t , for electron density $n = 1.6$ (since there are eight electrons for either $3d^6 4s^2$ Fe atom in 10 $3d$ spin channels) with (a) $U/t = 2$, and (b) $U/t = 6$. The ground state is determined by comparing energies of paraelectric and ferroelectric phases in the parameter space. For narrower charge-transfer gap or softer bond stiffness, FE structure becomes the ground state, signifying strong exchange gain surpasses distortive punishments. For this one-band model, repulsive U weakens the exchange interaction by breaking the exchange pairing, characterized by increased magnetic moment [Fig. 4(c)] and diminishes the bonus from charge-transfer gap narrowing, and thus reduces the FE phase zone at certain κ/t . Alternately, exchange energy can be inferred by the area of magnetic lag between ferroelectric and paraelectric phases [see meshed patterns in Fig. 4(d)], which

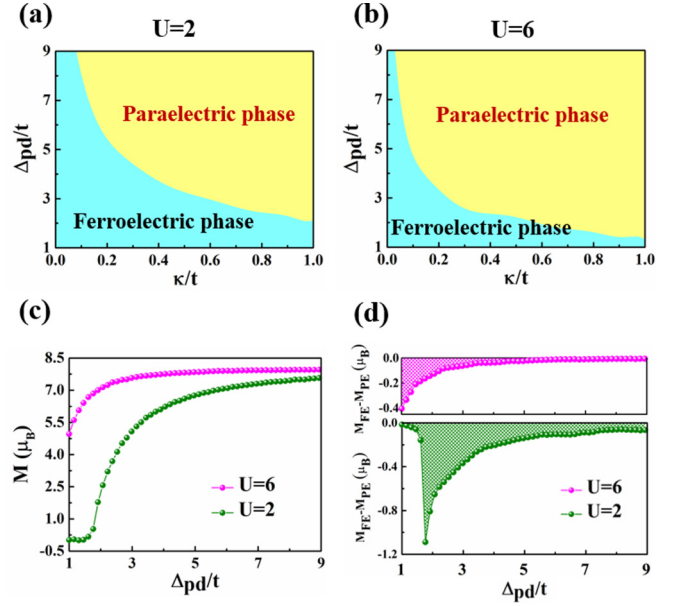


FIG. 4. Phase diagram varying κ/t and Δ_{pd}/t for (a) $U/t = 2$ and (b) $U/t = 6$. Magnetic moment (per site) of ferroelectric phase (c) and differential magnetic moment (per site) of ferroelectric versus paraelectric phase (d) from the model.

also decreases with strong U . Thus, a significant exchange interaction with narrow Δ_{pd} results in a magnetically induced ferroelectric.

C. DFT + U scheme

Beyond the above single-band picture, first-principles GGA + U scheme invokes realistic many-body exchange-correlation interactions as an analog of Hartree-Fock approximation, as well as multiorbital effects. Our proposal that the semicovalent superexchange mechanism contributes to the ferroelectricity of BFO is exactly based on its following peculiarities: (i) antiferromagnetic superexchange interaction is maximal in the half-filling Fe $t_{2g}^3 e_g^2$ configuration [70,71]; (ii) the characteristic of charge-transfer insulators with the band gap constituted by the Fe $3d$ -O $2p$ orbital overlap is a signature of strong interatomic hybridization. These peculiarities are fully described by GGA + U scheme. As depicted in GGA + U density of states (DOS), for both $R3c$ and paraelectric $R\bar{3}c$ BFO, the exchange splitting from strong U in d shell is larger than crystal-field splitting Δ_{CF} , mediating a high-spin $t_{2g}^3 e_g^2$ state. Besides, strong intraband electron-electron correlation further splits occupied spin-up t_{2g} and e_g into upper and lower Hubbard bands. Remarkably, the onset of ferroelectricity features t_{2g}^* spectral transfer from LUMO to HOMO [LUMO: lowest unoccupied molecular orbital, HOMO: highest occupied molecular orbital, encircled in Fig. 5(a)], and the formation of A_{1g} HOMO states with even parity [Fig. 5(b)]. Also, the calculated Fe-O charge-transfer gap Δ_{CT} is smaller than exchange-splitting gap [4.61 eV for $p-t_{2g}^*$ states, as compared with 6.06 eV (t_{2g}) and 6.90 eV (e_g), respectively], corroborating the formation of singlet states. To display this magnetically driven ferroelectric, we alter antiferromagnetic pairing via magnetic multiples through external magnetic

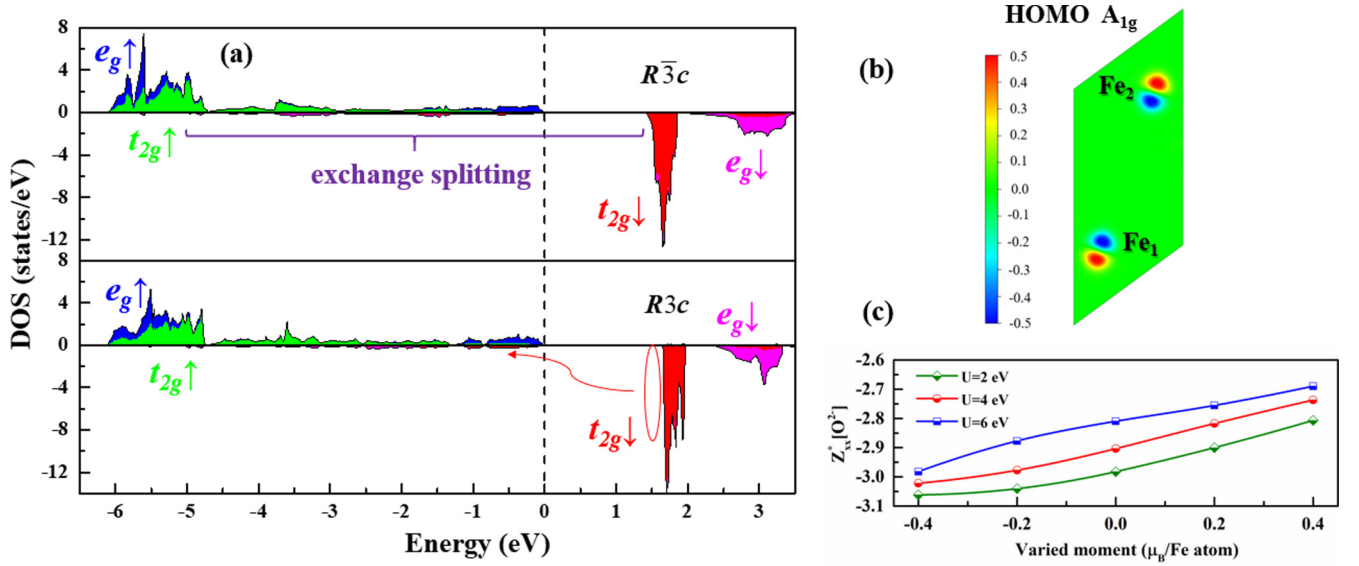


FIG. 5. GGA + U electronic structure of BFO in 10-atom G -type antiferromagnetic unit cell. (a) DOS of each Fe atom for $R\bar{3}c$ (top panel) and $R3c$ (bottom panel) structure, respectively. Zero of energy is set at GGA + U Fermi energies. (b) Projected spin-resolved charge isosurface [(-110) plane] of hybrid A_{1g} HOMO between adjacent Fe and O atoms. Note that singlet A_{1g} state features odd-spin and even-parity characters. (c) Born effective charge Z_{xx}^* of oxygen anion vs varied moment induced by external magnetic field.

field, and calculate the Born effective charge Z_{xx}^* of oxygen anion, whose anomalous enhancement features ferroelectricity [72,73]. Figure 5(c) shows enhanced Z_{xx}^* (versus nominal charge of -2) with decreasing moment on Fe ions through covalent exchange pairing, corroborating antiferromagnetic pairing's facilitation to the formation of singlet states and thus ferroelectricity in Fe $3d^5$ multiorbital manifold. Therefore, the semicovalent superexchange mechanism embraces magnetism in non- d^0 systems and renders BFO a magnetically driven ferroelectric.

D. Electronic structure and manipulatable hybridization

Precedingly established are the crucial ingredients, i.e., narrow renormalized Δ_{pd} (*viz.*, Δ_{CT}) and proper U in FE semicovalent superexchange mechanism. The Coulomb scale U , albeit sensitive to electron delocalization, is hardly directly manipulatable due to its intra-atomic on-site nature. We alternatively tune the bare charge transfer Δ_{pd} , using our OSEP method, which is usually responsive to experimental stimuli.

Figure 6 shows the spin-polarized PDOS for $R3c$ BFO, within a G -type antiferromagnetic solution. Localized Bi $6s$ states deeply locate around -10 eV, but slightly distributed in energy window (-6 eV, 0 eV) in hybridization with Bi $6p$ states due to the broken parity confinement of s - p orbital hybridization and concomitant FE distortion, i.e., stereochemical activity of $6s^2$ lone-pair electrons [60]. The Bi $6p$, O $2p$, and Fe $3d$ states are entangled with close energy levels and overlap bandwidths, indicating possible covalent hybridization among these states. We further tune the individual Fe $3d$ orbital, equivalently the bare charge transfer Δ_{pd} by OSEP method and up(down)-shifting Fe $3d$ in(de)-creases Δ_{pd} , to judge the relationships from changes. We ascertain the Fe-O covalency by the coincidentally sharper (lower) and narrower (broader) peak of Fe $3d$ and O $2p$ states with up(down)-shifting of Fe $3d$ state, resembling the crossover of energy dispersion

from isolated atoms to covalent band limit. Also, magnetic moments from unpaired O's $2p$ shell increase (0.036, 0.059, 0.107 μ_B) with Fe $3d$ down-shifting, signaling the creation of ligand hole featuring strong p - d charge transfer (see encircled region in PDOS) and semicovalent superexchange interaction. Thus, a possible hopping route for semicovalent superexchange includes ligand holes [74]:

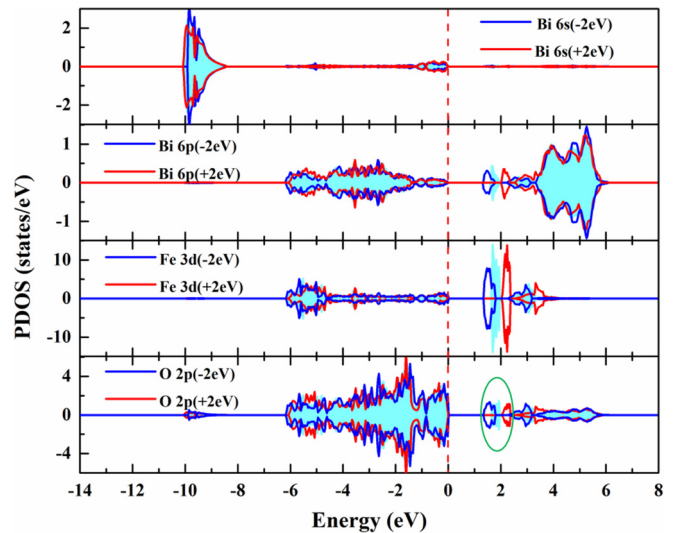
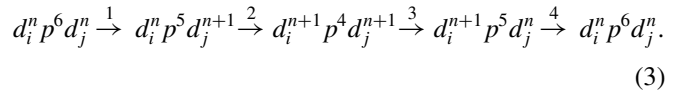


FIG. 6. PDOS for Bi $6s$, Bi $6p$, Fe $3d$, and O $2p$ with up(down)-shifting Fe $3d$ by 2 eV in $R3c$ BFO. The Fermi level is set at zero energies (vertical dashed lines), and pristine PDOS are depicted as shaded plots.

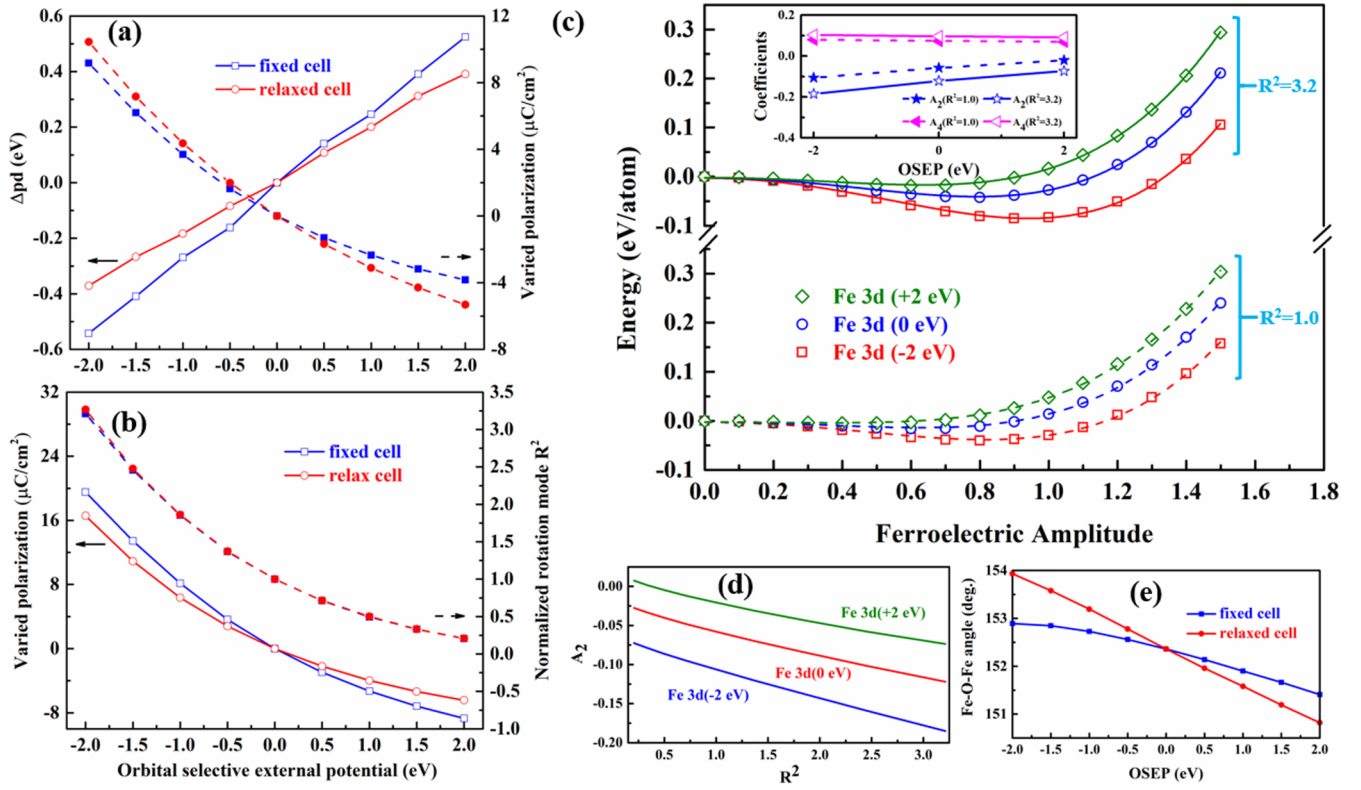


FIG. 7. Couplings of FE and rotation modes mediated by hybridization. The Δ_{pd} and displacive polarization (a), and rotation amplitude (b) within two relaxation strategies. The rotation and polar tilting modes of FeO_6 are included in (b). (c) Total energy as a function of the FE amplitude (intermediate FE displacements divided by spontaneous FE displacements) under different external potentials, with fixed rotation R^2 modes and lattice vectors of $R3c$ BFO. Symbols and line represent DFT results and their fit by the Landau-Ginzburg potentials, respectively. The inset in panel (c) shows resulting fitted parameters as a function of external potentials. (d) Coefficients A_2 vs rotational amplitude for different external potentials. (e) Fe-O-Fe bond angle vs external potentials under two relaxation strategies.

By contrast, Bi $6p$ states, albeit also affected by shifts of Fe $3d$ states, have no emergent magnetic moments. It is inferred that Bi $6p$ states hybridize indirectly with Fe $3d$ -O $2p$ bonding states; Bi's size effect tunes Fe-O-Fe bond angles, and thus enhances semicovalent superexchange interaction in BFO. As well, the reciprocity is self-evident with up (down)-shifting Bi $6p$ states or O $2p$ states due to the underlying hybridization (not shown).

We also confirm resultant ferroelectricity from semicovalent superexchange interaction in BFO by tuning Δ_{pd} . As mentioned above, the $R3c$ BFO lattice features collective FE displacive mode and antiphase oxygen octahedral FeO_6 rotations. All these modes mediate the Fe-O-Fe configurations, thus superexchange interaction and resultant ferroelectricity. Particularly, there exist competition and cooperation between these modes, ultimately strengthening or suppressing each other in perovskites [75–77]. We systematically study interplays of these unstable modes within semicovalent superexchange mechanism in two structural relaxation strategies. The fixed cell scheme refers to atomic relaxation with frozen lattice vectors while the relaxed cell scheme represents fully optimized symmetry-constrained lattice vectors. The strategies differ in an inclusion of hydrostatic rhombohedral strain or not. To produce Figs. 7(a) and 7(b), Fe's atomic displacements or O's rotations (also tilts) are exclusively optimized in each case. The equivalent atomic energy levels in

the band picture are estimated by band center $\varepsilon = \frac{\int_{-\infty}^{+\infty} n(\varepsilon)\varepsilon d\varepsilon}{\int_{-\infty}^{+\infty} n(\varepsilon) d\varepsilon}$, wherein $n(\varepsilon)$ denotes DOS at certain energy ε extracted from the DOS plots. Besides, we adopt a normalized dimensionless rotation mode R^2 , namely summed-squared oxygens' rotational displacements (except tilts) descending from $R\bar{3}c$ lattice and the unity is defined for pristine FE $R3c$ structure.

Figure 7(a) shows enhanced polarization of collective FE displacements with narrowing Δ_{pd} , when we down-shift Fe $3d$ states within both relaxation strategies. It accords with predictions of semicovalent superexchange mechanism. Also, the application of OSEP indeed allows one to manipulate charge-transfer gap in BiFeO_3 . The actual shifting energy of p - d band centers does not equal that applied, approximately varying linearly with external potential by a renormalized factor as ~ 0.2 (far less than unity and reconfirm strong p - d charge transfer). In Fig. 7(b), the amplitude of oxygen octahedral rotation R^2 becomes larger, along with consistent polarization enhancement with narrowing Δ_{pd} , indicating its cooperative nature with FE mode in BFO. Hydrostatic rhombohedral strain does not qualitatively switch the trend of all above, but differs a little. For FE mode under the strain [i.e., fixed cell scheme, Fig. 7(a)], p - d band center varies more dramatically but polarization does not as compared with the relaxed cell scheme, implying the strain narrows Δ_{pd} yet with destructions to ferroelectricity. It typically can be understood by the fact

that short-range repulsions (favoring a paraelectric state) increase more rapidly than long-range FE interactions as strain increases [78,79]. However, by invoking antiferrodistortive FeO_6 modes (inert to strain) and polar O's tilting modes, FE instability surpasses repulsive energy, as evidenced by drastic changes of polarization under the strain.

E. Phenomenological analysis

To shed further light on the cooperative nature of FE and antiferrodistortive modes driven by semicovalent superexchange mechanism, we introduce a Landau-Ginzburg potential in 10-atom G -type antiferromagnetic unit cell [77]. For the sake of simplicity, strain degree of freedom is not explicitly included. The phenomenological potential can thus be expressed by symmetry [77] as $E(u, R^2) = A_2(R^2)u^2 + A_4(R^2)u^4 + E(R^2)$ up to fourth order in displacive FE mode, where u and R^2 denote amplitudes of displacive ferroelectricity and reduced antiphase rotation, respectively. The coupling coefficients $A_{2i} = A_{u^{2i}} + A_{u^{2i}R^2}R^2$ ($i = 1, 2$) include the second order in rotation mode, with parameters A to be fitted from first-principles calculations. In Fig. 7(c), the total energy of $R3c$ phases under different external potentials is plotted as a function of the displacive FE amplitude at two fixed rotation amplitudes. For both modes, the minimal of energy curve goes down and moves towards larger displacive FE amplitude with down-shifting Fe $3d$ states, indicating narrow Δ_{pd} promotes FE instability. And, larger rotation amplitude enhances FE modes. To reveal the underlying coupling modes, we numerically fit the above Landau-Ginzburg potentials to our DFT results and extract the A parameters. As depicted in the inset of Fig. 7(c), A_2 is susceptible to Δ_{pd} and thus mainly of magnetic origin, while rigid A_4 (almost intact) is of steric origin. We extract dominant u^2R^2 coupling term from linear relation of A_2 versus R^2 in Fig. 7(d). The negative sign of $A_{u^2R^2}$ signifies collaborative nature of FE instability and octahedral rotation. Note that different from the cooperativity from the u^2R^4 term and its steric origin [77], our first-order u^2R^2 coupling microscopically stems from stretch effects of Fe-O-Fe angle with large rotation modes [Fig. 7(e)] and concomitant enhancement of superexchange interaction. Therefore, we conclude that via collaborative antiferrodis-

tortive FeO_6 modes, semicovalent superexchange mechanism surpasses repulsions for ferroelectricity to occur in BFO.

IV. CONCLUSION

We have identified the ferroelectricity of lone-pair electrons, which originates from nominal s^2 electrons' instability with strong hybridizations among Bi's $6s$ and $6p$ as well O's $2p$ states. The well-believed lone-pairs FE mechanism, however, cannot explain the overall polarization of BFO. We thus propose an intrinsic magnetoelectric coupling mechanism from semicovalent superexchange interaction in p - d charge-transfer insulators, and demonstrate it in representative room-temperature multiferroic BFO. We have identified its key ingredients in BFO as follows: (a) half-filling $3d^5$ states with strong semicovalent superexchange interaction and (b) stereochemical activity of Bi lone-pair electrons, triggering strong superexchange interaction in narrow p - d charge-transfer regime. The magnetically induced ferroelectricity occurs via collaborative u^2R^2 coupling with antiferrodistortive FeO_6 modes. This mechanism can also elucidate the concurrent \mathbf{P} and \mathbf{M} enhancement in supertetragonal BFO with strengthened antiferromagnetic superexchange in 180° Fe-O-Fe bond configurations with FE-active e_g^* orbital, and unveil underrated strong magnetically driven ferroelectricity in BFO, even covering a broad category of collinear magnets. Within the magnetoelectric scenario, the magnetically driven ferroelectricity vanishes as magnetic order disappears, thus ferroelectricity anomaly is also predicted at the antiferromagnetic-paramagnetic transition of BFO, which appeals to in-depth experiments. Furthermore, its susceptibility to charge-transfer gap renders the magnetoelectric coupling manipulatable to hybridization engineering.

ACKNOWLEDGMENTS

This work was supported by the National Key Research and Development Program of China (Grant No. 2017YFA0303403), Shanghai Science and Technology Innovation Action Plan (Grant No. 19JC1416700), the NSF of China (Grants No. 11774092 and No. 51572085), and ECNU Multifunctional Platform for Innovation.

-
- [1] J. Wang, J. B. Neaton, H. Zheng, V. Nagarajan, S. B. Ogale *et al.*, *Science* **299**, 1719 (2003).
 - [2] T. Kimura, T. Goto, H. Shintani, K. Ishizaka, T. Arima, and Y. Tokura, *Nature (London)* **426**, 55 (2003).
 - [3] D. V. Efremov, J. Van den Brink, and D. I. Khomskii, *Nat. Mater.* **3**, 853 (2004).
 - [4] M. Fiebig, *J. Phys. D: Appl. Phys.* **38**, R123 (2005).
 - [5] C. G. Duan, S. S. Jaswal, and E. Y. Tsymlal, *Phys. Rev. Lett.* **97**, 047201 (2006).
 - [6] W. Eerenstein, N. D. Mathur, and J. F. Scott, *Nature (London)* **442**, 759 (2006).
 - [7] R. Ramesh and N. A. Spaldin, *Nat. Mater.* **6**, 21 (2007).
 - [8] S. W. Cheong and M. Mostovoy, *Nat. Mater.* **6**, 13 (2007).
 - [9] D. Khomskii, *Physics* **2**, 20 (2009).
 - [10] K. F. Wang, J. M. Liu, and Z. F. Ren, *Adv. Phys.* **58**, 321 (2009).
 - [11] N. A. Spaldin, S. W. Cheong, and R. Ramesh, *Phys. Today* **63**(10), 38 (2010).
 - [12] J. Ma, J. M. Hu, Z. Li, and C. W. Nan, *Adv. Mater.* **23**, 1062 (2011).
 - [13] Y. Tokura, S. Seki, and N. Nagaosa, *Rep. Prog. Phys.* **77**, 076501 (2014).
 - [14] S. Dong, J.-M. Liu, S.-W. Cheong, and Z. Ren, *Adv. Phys.* **64**, 519 (2015).
 - [15] J. M. Hu, L. Q. Chen, and C. W. Nan, *Adv. Mater.* **28**, 15 (2016).
 - [16] M. Fiebig, T. Lottermoser, D. Meier, and M. Trassin, *Nat. Rev. Mater.* **1**, 16046 (2016).
 - [17] N. A. Spaldin, *MRS Bull.* **42**, 385 (2017).
 - [18] N. A. Spaldin and R. Ramesh, *Nat. Mater.* **18**, 203 (2019).
 - [19] C. Lu, M. Wu, L. Lin, and J.-M. Liu, *Natl. Sci. Rev.* **6**, 653 (2019).

- [20] T. Hu and E. J. Kan, *Wires Comput. Mol. Sci.* **9**, e1409 (2019).
- [21] G. Catalan and J. F. Scott, *Adv. Mater.* **21**, 2463 (2009).
- [22] N. A. Hill, *J. Phys. Chem. B* **104**, 6694 (2000).
- [23] D. I. Khomskii, *J. Magn. Magn. Mater.* **306**, 1 (2006).
- [24] I. B. Bersuker, *Phys. Rev. Lett.* **108**, 137202 (2012).
- [25] Q. He, Y. H. Chu, J. T. Heron, S. Y. Yang, W. I. Liang *et al.*, *Nat. Commun.* **2**, 225 (2011).
- [26] G. W. Watson, S. C. Parker, and G. Kresse, *Phys. Rev. B* **59**, 8481 (1999).
- [27] A. Walsh, D. J. Payne, R. G. Egdell, and G. W. Watson, *Chem. Soc. Rev.* **40**, 4455 (2011).
- [28] J. M. Rondinelli, A. S. Eidelson, and N. A. Spaldin, *Phys. Rev. B* **79**, 205119 (2009).
- [29] C. Ederer, T. Harris, and R. Kovacic, *Phys. Rev. B* **83**, 054110 (2011).
- [30] L. Weston, X. Y. Cui, S. P. Ringer, and C. Stampfl, *Phys. Rev. B* **93**, 165210 (2016).
- [31] W. Cochran, *Phys. Rev. Lett.* **3**, 412 (1959).
- [32] W. Cochran, *Adv. Phys.* **9**, 387 (1960).
- [33] V. L. Ginzburg, *Zh. Eksp. Teor. Fiz.* **15**, 739 (1945).
- [34] P. W. Anderson, in *Fizika Dielektrikov* (Acad. Nauk SSSR, Moscow, 1959), p. 290.
- [35] L. Landau and E. M. Lifshitz, *Statistical Physics*, Part I, 3rd ed. (Butterworth-Heinemann, Oxford, 1994), Vol. 5, p. 446.
- [36] P. Barone, S. Kanungo, S. Picozzi, and T. Saha-Dasgupta, *Phys. Rev. B* **84**, 134101 (2011).
- [37] X. Wan, H. C. Ding, S. Y. Savrasov, and C. G. Duan, *Sci. Rep.* **6**, 22743 (2016).
- [38] P. W. Anderson, *Phys. Rev.* **115**, 2 (1959).
- [39] W. A. Harrison, *Electronic Structure and the Properties of Solids: The Physics of the Chemical Bond* (Dover Publications, 1989).
- [40] A. Bolens, *Phys. Rev. B* **98**, 125135 (2018).
- [41] I. V. Solovyev, *Phys. Rev. B* **95**, 214406 (2017).
- [42] J. H. Lee and R. S. Fishman, *Phys. Rev. Lett.* **115**, 207203 (2015).
- [43] J. B. Goodenough, *Magnetism and the Chemical Bond* (Interscience Publishers, New York, 1963).
- [44] P. E. Blöchl, *Phys. Rev. B* **50**, 17953 (1994).
- [45] G. Kresse and D. Joubert, *Phys. Rev. B* **59**, 1758 (1999).
- [46] G. Kresse and J. Furthmüller, *Comput. Mater. Sci.* **6**, 15 (1996).
- [47] J. P. Perdew, K. Burke, and M. Ernzerhof, *Phys. Rev. Lett.* **77**, 3865 (1996).
- [48] S. L. Dudarev, G. A. Botton, S. Y. Savrasov, C. J. Humphreys, and A. P. Sutton, *Phys. Rev. B* **57**, 1505 (1998).
- [49] M. Gajdoš, K. Hummer, G. Kresse, J. Furthmüller, and F. Bechstedt, *Phys. Rev. B* **73**, 045112 (2006).
- [50] S. Baroni and R. Resta, *Phys. Rev. B* **33**, 7017 (1986).
- [51] R. D. King-Smith and D. Vanderbilt, *Phys. Rev. B* **47**, 1651 (1993).
- [52] D. Vanderbilt and R. D. King-Smith, *Phys. Rev. B* **48**, 4442 (1993).
- [53] R. Resta, *Rev. Mod. Phys.* **66**, 899 (1994).
- [54] A. Togo and I. Tanaka, *Scr. Mater.* **108**, 1 (2015).
- [55] G. Pizzi, V. Vitale, R. Arita, S. Blügel, F. Freimuth *et al.*, *J. Phys.: Condens. Matter* **32**, 165902 (2020).
- [56] K. Momma and F. Izumi, *J. Appl. Crystallogr.* **44**, 1272 (2011).
- [57] Y. Du, H.-C. Ding, L. Sheng, S. Y. Savrasov, X. Wan, and C.-G. Duan, *J. Phys.: Condens. Matter* **26**, 025503 (2013).
- [58] X. Wan, J. Zhou, and J. Dong, *EPL* **92**, 57007 (2010).
- [59] X. Wan, J. Dong, and S. Y. Savrasov, *Phys. Rev. B* **83**, 205201 (2011).
- [60] Y. Shen, J. Cai, H. C. Ding, X. W. Shen, Y. W. Fang, W. Y. Tong, X. G. Wan, Q. Zhao, and C. G. Duan, *Adv. Theory Simul.* **2**, 1900029 (2019).
- [61] R. A. Wheeler and P. P. Kumar, *J. Am. Chem. Soc.* **114**, 4776 (1992).
- [62] S. Suehara, P. Thomas, A. P. Mirgorodsky, T. Merle-Méjean, J. C. Champarnaud-Mesjard *et al.*, *Phys. Rev. B* **70**, 205121 (2004).
- [63] J. X. Zhang, Q. He, M. Trassin, W. Luo, D. Yi, M. D. Rossell, P. Yu, L. You, C. H. Wang, C. Y. Kuo *et al.*, *Phys. Rev. Lett.* **107**, 147602 (2011).
- [64] M. Wu and P. Jena, *Wiley Interdiscip. Rev. Comput. Mol. Sci.* **8**, e1365 (2018).
- [65] D. D. Khalyavin, R. D. Johnson, F. Orlandi, P. G. Radaelli, P. Manuel, and A. A. Belik, *Science* **369**, 680 (2020).
- [66] H.-C. Ding, S.-Q. Shi, W.-H. Tang, and C.-G. Duan, *J. Adv. Dielectr.* **01**, 179 (2012).
- [67] A. Paul, A. Mukherjee, I. Dasgupta, A. Paramekanti, and T. Saha-Dasgupta, *Phys. Rev. Lett.* **122**, 016404 (2019).
- [68] J. R. Schrieffer and P. A. Wolff, *Phys. Rev.* **149**, 491 (1966).
- [69] Y. Claveau, B. Arnaud, and S. Di Matteo, *Eur. J. Phys.* **35**, 035023 (2014).
- [70] J. Kanamori, *J. Phys. Chem. Solids* **10**, 87 (1959).
- [71] J. B. Goodenough, *J. Phys. Chem. Solids* **6**, 287 (1958).
- [72] W. Zhong, R. D. King-Smith, and D. Vanderbilt, *Phys. Rev. Lett.* **72**, 3618 (1994).
- [73] P. Ghosez, J.-P. Michenaud, and X. Gonze, *Phys. Rev. B* **58**, 6224 (1998).
- [74] D. Khomskii, *Transition Metal Compounds* (Cambridge University Press, Cambridge, 2014).
- [75] I. A. Kornev, L. Bellaiche, P. E. Janolin, B. Dkhil, and E. Suard, *Phys. Rev. Lett.* **97**, 157601 (2006).
- [76] W. Zhong and D. Vanderbilt, *Phys. Rev. Lett.* **74**, 2587 (1995).
- [77] T. Gu, T. Scarbrough, Y. R. Yang, J. Iniguez, L. Bellaiche, and H. J. Xiang, *Phys. Rev. Lett.* **120**, 197602 (2018).
- [78] E. Bousquet and P. Ghosez, *Phys. Rev. B* **74**, 180101(R) (2006).
- [79] G. Samara, T. Sakudo, and K. Yoshimitsu, *Phys. Rev. Lett.* **35**, 1767 (1975).